

## Morphology of femtosecond-laser-ablated borosilicate glass surfaces

Adela Ben-Yakar<sup>a)</sup> and Robert L. Byer

*Applied Physics Department, Ginzton Lab, Stanford University, California 94305*

Anthony Harkin, Jacqueline Ashmore, and Howard A. Stone

*Division of Engineering and Applied Sciences, Harvard University, Cambridge, Massachusetts 02138*

Mengyan Shen and Eric Mazur

*Department of Physics and Division of Engineering and Applied Sciences, Harvard University, Cambridge, Massachusetts 02138*

(Received 11 April 2003; accepted 25 August 2003)

We study the morphology of borosilicate glass surface machined by femtosecond laser pulses. Our observations show that a thin rim is formed around ablated craters after a single laser pulse. When multiple laser pulses are overlapped, the crater rims also overlap and produce a surface roughness. The rim appears to be a resolidified splash from a molten layer generated during the ablation process. We estimate that this molten layer is a few micrometers thick and exists for a few microseconds. During this melt lifetime, forces acting on the molten layer move it from the center to the edge of the crater. © 2003 American Institute of Physics. [DOI: 10.1063/1.1619560]

Microchannels fabricated on glass have a growing importance in the miniaturization of microfluidic devices for chemical and biological micrototal-analysis systems.<sup>1,2</sup> In most cases, chips are fabricated using traditional multilayer and multistep photolithographic techniques. Laser micromachining using ultrashort pulses offers a single-step method for direct writing of microchannels in glass.<sup>3–6</sup> Using this laser ablation technique, it is possible to fabricate geometries with variable depth and high aspect ratio that cannot be achieved through traditional microlithographic techniques.

Recently, ultrashort laser pulses have been used to machine microchannels in transparent glasses such as borosilicate glass and fused silica.<sup>3,6</sup> However, the authors report that micrometer-size features are formed inside the channels and that the walls of the ablated surfaces are not smooth (an example is shown in Fig. 1). To better control the micromachining process using ultrashort laser pulses it is necessary to understand the formation mechanism of these small surface features. In this letter, we investigate the surface morphology of single shot ablated craters and show how the interaction of multiple overlapping craters leads to surface roughness.

We carried out experiments on borosilicate glass (1.1 mm thick, Precision Glass and Optics, Ltd.), also known as Borofloat™ and Corning 7740, whose chemical composition is 81% SiO<sub>2</sub>, 13% B<sub>2</sub>O<sub>3</sub>, 2% Al<sub>2</sub>O<sub>3</sub>, 4% Na<sub>2</sub>O. The substrates were cleaned ultrasonically with alcohol before the experiments. After laser ablation, the debris was removed by placing the sample in an ultrasonic bath with a 0.5 M sodium hydroxide (NaOH) solution (a very weak etchant) for about 20 min.

We irradiated the glass samples with near-infrared (780–800 nm) femtosecond (100–200 fs) laser pulses from a regeneratively amplified Ti:sapphire laser. The surface of the sample was positioned normal to the direction of the incident

beam. Following irradiation, the samples were analyzed with a scanning electron microscope (SEM).

Figure 1 shows the surface morphology of a microchannel produced with 200 fs pulses at an average laser fluence of 0.12 J/mm<sup>2</sup>. The laser beam was delivered to the surface by a long working distance objective lens (Mitutoya, 5×, numerical aperture=0.14) attached to a microscope. The focused beam has a Gaussian spatial beam profile with a 1/e<sup>2</sup> diameter of 11.8 μm at the surface of the target. We performed the experiment in a vacuum chamber at a pressure below 10<sup>-4</sup> mbar. The channel was produced by moving the sample with a scanning speed of 1.5 mm/s at a 1 kHz laser repetition rate, so that the average number of pulses overlapping on the same spot was about 6. The resulting channel has a 9.6 μm width and about 2.5 μm depth. The most pronounced feature of the microchannel surface morphology shown in Fig. 1 is the micrometer-scale roughness.

To better understand the source of this surface roughness we studied how the glass surface responds to irradiation with sparsely overlapped single laser pulses. Figure 2 shows SEM

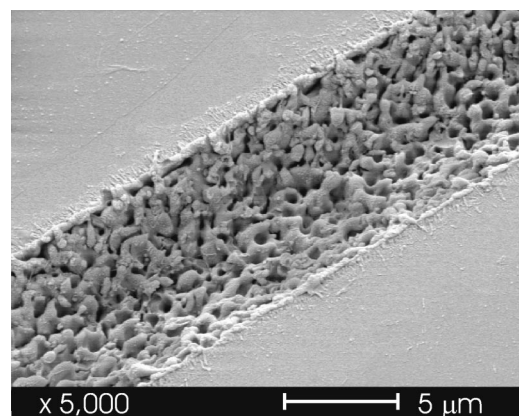


FIG. 1. Surface morphology of a microchannel fabricated on borosilicate glass using 780 nm and 200 fs laser pulses. The channel is 9.6 μm wide and about 2.5 μm deep. The number of overlapping pulses was about  $N=6$  and the average laser fluence was  $F_0=0.12$  J/mm<sup>2</sup>.

<sup>a)</sup>Electronic mail: adela@stanford.edu

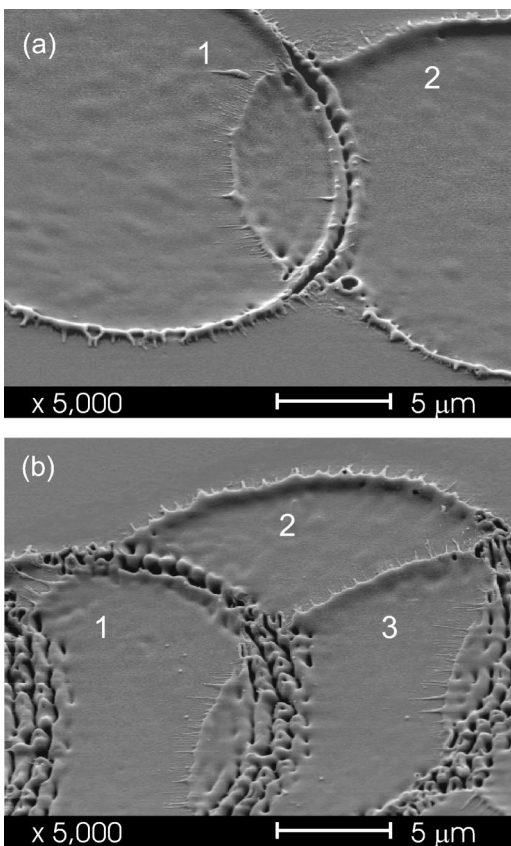


FIG. 2. SEM images of crater rims generated by overlapping laser pulses (a) two pulses and (b) three pulses of 800 nm and 100 fs. The laser fluence was  $F_0 = 0.34 \text{ J/mm}^2$ . The numbers correspond to the order of the incident laser pulses.

images of overlapping craters produced by single 100 fs laser pulses at an average laser fluence of  $0.34 \text{ J/mm}^2$ . The laser was focused with a 250 mm focal length lens to a spot size of about  $30 \mu\text{m}$ . We performed these experiments in air at atmospheric pressure. Two features stand out in this figure. First, a thin rim surrounds the craters. Second, when another pulse irradiates a previously formed crater, a new rim is formed at a distance approximately equal to the laser wavelength- $\lambda$  away from the previous rim. This suggests that diffraction of light plays a role in the formation of multiple rims.<sup>7</sup>

Figure 2(a) clearly shows that the second rim continuously follows the first one on the ablated side of the first crater. The second laser beam diffracts through the edges of a previously formed crater and therefore creates a modulated light intensity at the bottom of the crater due to the interference of the diffracted light in the near field. The second rim may therefore be a result of the modulated intensity distribution of the second laser pulse near the edges.

When a third pulse irradiates two previously overlapping craters, as shown in Fig. 2(b), micrometer-scale organized features appear along the rim. As the number of overlapping pulses increases, the interplay between rim formation and diffraction results in the surface microfeatures observed in Fig. 1. Let us next examine the formation of a single rim surrounding an ablation crater.

Figure 3 shows a SEM image of a crater generated with a single 100 fs laser pulse at a fluence of  $0.34 \text{ J/mm}^2$ . The image shows a circular rim that is raised 50–100 nm above

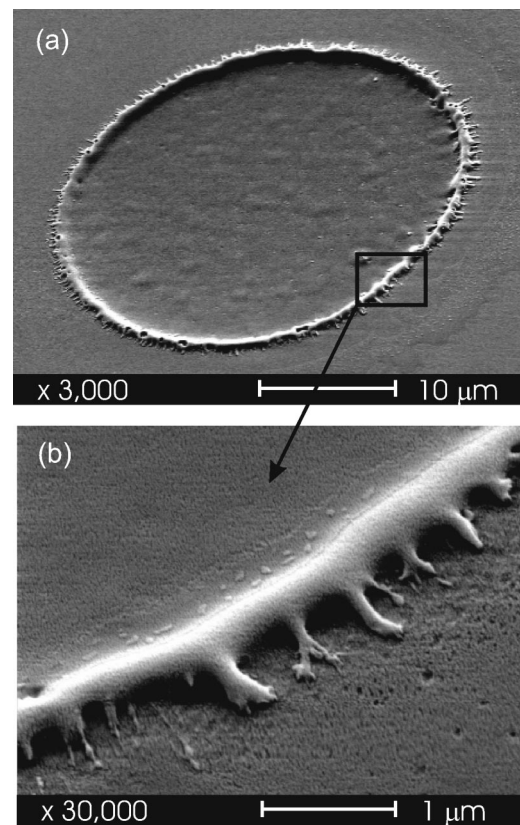


FIG. 3. SEM images of a crater generated with a single 800 nm and 100 fs laser pulse. (a) The whole crater at  $3000\times$  magnification and (b) a higher resolution SEM image ( $30\,000\times$  magnification) focused on the rim formed around the crater. The laser fluence was  $F_0 = 0.34 \text{ J/mm}^2$ .

the surface and that surrounds a smooth center. Part of the rim is shown at higher magnification in Fig. 3(b). This image suggests that the rim is a resolidified splash of a molten layer generated during the ablation process.

In ultrafast laser ablation, the rapid energy deposition in the material allows material removal before significant heating of the bulk material occurs. Nevertheless, as we demonstrate next, enough energy is deposited in the undamaged part of the material to create a shallow molten zone below the ablated area. If the melt lifetime is long enough, forces acting on the fluid can drive molten material from the center to the edges of the crater.<sup>8</sup> To estimate the thickness and the lifetime of the molten layer, we next analyze the absorption of the laser energy and its dissipation through a one-dimensional heat conduction calculation.

In dielectric materials, incident laser energy is absorbed through nonlinear processes (multiphoton and avalanche ionization).<sup>9,10</sup> Perry *et al.*<sup>9</sup> showed that far above the ablation threshold fluence ( $F > 5 - 10F_{\text{th}}$  where  $F_{\text{th}} = 0.02 \text{ J/mm}^2$  for fused silica), a large portion of the energy is reflected back from the sample. At a laser irradiance of  $10^{12} \text{ W/mm}^2$  they calculate the reflectance of a fused silica surface to be around 70%. We used a similar laser irradiance, and therefore we assume that on average 30% of the incident energy is absorbed by the borosilicate glass.

The laser energy is absorbed by electrons and then transferred to the lattice on the time scale of a few picoseconds, after which heat diffusion into the material begins. Simultaneously, the ionized material is removed away from the sur-

face in the form of an expanding high pressure plasma. Numerical simulations<sup>11</sup> of the fluid and thermal dynamics of a laser-induced plasma on an aluminum target irradiated with 100 ps laser pulses show that a few microseconds after irradiation, about 70% of the absorbed energy is used by the expanding plasma to move the ambient gas. About 20% of the absorbed energy is lost in radiation and only 10% of it remains in the target as thermal energy.

Assuming a similar energy partition in our experiments we can estimate that less than 3% of the incident laser energy (i.e., 10% of the absorbed energy) is available to heat the undamaged material. Therefore, at an incident laser fluence of 0.34 J/mm<sup>2</sup> (Figs. 2 and 3) less than 0.01 J/mm<sup>2</sup> goes into heating of the material. Because glass does not have a latent heat of melting, all of this energy goes into melting. We can calculate the average melting depth,  $h_m$ , from  $h_m \approx F_a/T_m\rho C_p$ , where  $F_a=0.01$  J/mm<sup>2</sup> is the portion of the absorbed laser fluence that goes into heating,  $\rho=2.23 \times 10^3$  kg/m<sup>3</sup><sup>12</sup> is the density,  $C_p=1250$  J/kg K<sup>13</sup> is the specific heat at an average temperature of  $T=900$  K, and  $T_m=1500$  K<sup>12</sup> is the working point of glass, defined as the temperature at which the glass can be easily formed and sealed. This calculation yields a molten layer of thickness  $h_m \approx 2.4$   $\mu$ m at the irradiated surface below the expanding plasma.

The lifetime of this molten region depends on how quickly the energy dissipates into the bulk. For one-dimensional heat conduction, the heat diffusion depth is approximately given by  $\ell \approx \sqrt{Dt}$ , where  $D=k/\rho C_p$  is the thermal diffusivity. For an average temperature around 900 K,  $D=1.6 \times 10^{-6}$  m<sup>2</sup>/s<sup>13</sup> and we estimate that it takes about  $h_m^2/D \approx 3.6$   $\mu$ s to melt the 2.4- $\mu$ m-thick layer, after which resolidification begins. Therefore, we expect a characteristic melt lifetime of the order of several microseconds, including the melting and resolidification processes. A detailed calculation yields results consistent with these order-of-magnitude estimates.<sup>14</sup>

During this melt lifetime, forces acting on the ablated surface move the molten material from the center of the crater to the edge depositing a thin rim around the ablated area. Two forces affect the surface of the molten layer: (1) thermocapillary forces (Marangoni flow)<sup>15</sup> and (2) hydrodynamic forces exerted by the plasma above the surface.<sup>16</sup>

Thermocapillary flow is induced by the temperature gradient on the surface following the Gaussian beam intensity profile of the laser. This temperature gradient creates surface tension gradients that drives material from the hot center to the cold periphery. This is true in most materials where the surface tension,  $\gamma$ , decreases as the fluid gets hotter ( $d\gamma/dT < 0$ ). However, in the case of borosilicate glass  $d\gamma/dT$  is positive.<sup>17</sup> This means that the thermocapillary flow in laser irradiated glass surfaces would actually drive fluid from the cold periphery to the hot center of the melt contrary to what is observed in our experiments.

The flow is most likely caused by hydrodynamic forces due to pressure gradients caused by the plasma that is formed above the molten surface. The plasma pressure initially is

very high, typically millions of atmospheres and drops to  $\approx 10$  atm during the first microsecond of its expansion.<sup>18</sup> The pressure gradients are particularly large at the edges of the ablated crater because of the plasma/air interface. Because of these large pressure gradients, we might expect a very fast rise of a thin rim at the edges of the melted surface. The very thin tendrils emanating from the outside of the rim might therefore be a result of a very fast rising rim, which became unstable and subsequently resolidified on the surface. In a follow-up study, we performed a theoretical analysis to model the free-surface evolution of the molten material.<sup>14</sup> For the conditions indicated earlier, the results predict that the time necessary for a pressure-driven flow to form a rim is of the same order of magnitude as the melt lifetime.

In conclusion, we investigated the origin of the surface roughness of femtosecond laser ablated borosilicate glass microchannels. We find that an interplay between light diffraction and flow of molten material cause the surface roughness. The morphology of the single-pulse ablated areas reveals the existence of an elevated rim surrounding smooth craters. From these observations, we suggest that a very thin melt zone (a few microns thick) exists during the ablation process and that during the melt lifetime (a few microseconds), the molten fluid moves from the center of the crater to the edge depositing a thin rim around the ablated area.

The work is supported by the TRW research fund and the Harvard NSEC. The authors gratefully acknowledge the contributions of Dr. Catherine Crouch to this investigation.

- <sup>1</sup>J. Voldman, M. L. Gray, and M. A. Schmidt, *Annu. Rev. Biomed. Eng.* **1**, 401 (1999).
- <sup>2</sup>D. J. Beebe, G. A. Mensing, and G. M. Walker, *Annu. Rev. Biomed. Eng.* **4**, 261 (2002).
- <sup>3</sup>S. Ameer-Beg, W. Perrie, S. Rathbone, W. Wright, J. Weaver, and H. Champoux, *Appl. Surface Phys.* **127–129**, 875 (1998).
- <sup>4</sup>Y. Li, K. Itoh, W. Watanabe, Y. Kazuhiro, D. Kuroda, J. Nishii, and Y. Jiang, *Opt. Lett.* **26**, 1912 (2001).
- <sup>5</sup>A. Marcinkevicius, S. Juodkazis, M. Watanabe, M. Miwa, S. Matsuo, H. Misawa, and J. Nishii, *Opt. Lett.* **26**, 277 (2001).
- <sup>6</sup>A. Ben-Yakar and R. L. Byer, *Proc. SPIE* **4637**, 212 (2002).
- <sup>7</sup>M. Born and E. Wolf, *Principles of Optics*, 7th ed. (Cambridge University Press, Cambridge, 1999).
- <sup>8</sup>A. Ben-Yakar, A. Harkin, J. Ashmore, M. Shen, E. Mazur, R. L. Byer, and H. A. Stone, *Proc. SPIE* **4977**, 335 (2003).
- <sup>9</sup>M. D. Perry, B. C. Stuart, P. S. Banks, M. D. Feit, V. Yanovsky, and A. M. Rubenchik, *J. Appl. Phys.* **85**, 6803 (1999).
- <sup>10</sup>C. B. Schaffer, A. Brodeur, and E. Mazur, *Meas. Sci. Technol.* **12**, 1784 (2001).
- <sup>11</sup>F. Vidal, S. Laville, B. Le Drogoff, T. W. Johnston, M. Chaker, O. Barthélemy, J. Margot, and M. Sabsabi, Annual meeting of OSA—Optical Society of America, 2001.
- <sup>12</sup>R. H. Doremus, *Glass Science*, 2nd ed. (Wiley, New York, 1994).
- <sup>13</sup>G. W. McLellan and E. B. Shand, *Glass Engineering Handbook*, 3rd ed. (McGraw-Hill, New York, 1984).
- <sup>14</sup>A. Ben-Yakar, A. Harkin, J. Ashmore, R. L. Byer, and H. A. Stone (unpublished).
- <sup>15</sup>T. Schwarz-Selinger, D. G. Cahill, S. C. Chen, S. J. Moon, and C. P. Grigoropoulos, *Phys. Rev. B* **64**, 155323 (1999).
- <sup>16</sup>V. N. Tokarev and A. F. H. Kaplan, *J. Phys. D* **32**, 1526 (1999).
- <sup>17</sup>W. D. Kingery, *J. Am. Ceram. Soc.* **42**, 6 (1959).
- <sup>18</sup>F. Vidal, S. Laville, T. W. Johnston, O. Barthélemy, M. Chaker, B. Le Drogoff, J. Margot, and M. Sabsabi, *Spectrochim. Acta, Part B* **56**, 973 (2001).